RSC Advances

PAPER

View Article Online
View Journal | View Issue

Cite this: RSC Adv., 2015, 5, 28454

Catalyst-dependent morphological evolution by interfacial stress in crystalline–amorphous core–shell germanium nanowires†

Nithin Devarajulu Palavalli,[a] Alireza Yaghoubi,[b] Chih-Chung Lai,[a] Chin-Che Tin,[cd] Ali Javey*[e] and Yu-Lun Chueh*[a]

Received 15th January 2015
Accepted 2nd March 2015

DOI: 10.1039/c5ra00888c

www.rsc.org/advances

Directing the morphological evolution of one-dimensional materials in order to tune their properties for a variety of practical applications in optical sensing and solar cells is an ongoing effort. Here, we establish a systematic method for exerting control over the morphology of nanowires (NWs) grown *via* a vapour–solid–solid (VSS) process from different metal catalysts. We use germanium, a technologically important material, to demonstrate how catalysts influence the axial growth rate of a crystalline core against the lateral vapour deposition of an amorphous shell which in turn deforms the NWs into straight, tapered or spiral geometries due to interfacial stress. Finite element method (FEM) and molecular dynamic (MD) simulations are further utilized to confirm the proposed mechanism of deformation in crystalline–amorphous core–shell NWs.

Introduction

The quantum size effect is sensitively dependent on the shape of nanostructures.[1,2] As a result, in recent years, considerable effort has been put toward understanding the detailed mechanism of growth and control of the morphology of nanomaterials. The specific technique that is employed for controlled synthesis and growth at the nanoscale can greatly vary based on the precursors as well as the intended application. For example, methods for directing the growth of nanocrystals by defect-induced secondary nucleation in iono-covalent materials[3] or enthalpy-specific plasmatic environments for materials which exhibit strong polymorphism have been recently reported.[4] From a practical standpoint, morphological modifications in NWs are particularly of interest.[5] In several studies, the improved anti-reflective properties due to the gradual reduction of the effective refractive index from the tip to the base of NWs have been shown to significantly differ for distinct morphologies.[6–8] Owing to their superior compatibility with the current fabrication techniques, silicon (Si) NWs have been a natural choice for nanoelectronic applications,[9,10] although Si-based devices because of the relatively large band gap of Si ($E_g \sim 1.12$ eV) suffer from poor responsivity in IR and NIR regimes where most transmission bands operate. For this reason, more recently, germanium (Ge) NWs have been studied as a potential replacement for Si NWs as the active material of nanoscale photodetectors operating at telecommunication frequencies.[11,12] With regard to other applications, especially in electronics, Ge due to its substantially higher mobility[13] and larger excitonic Bohr radius, which enables a more prominent quantum size effect[14] is a far more desirable candidate for high-performance devices.

However, both Si and Ge in their crystalline form are indirect band gap semiconductors and therefore do not efficiently absorb light at near band gap energies where phonon and photon (to conserve momentum and energy, respectively) need to simultaneously couple in order to give rise to a strong optical absorption. Meanwhile, it has been suggested that since a-Si does not essentially require a phonon interaction given its lack of long-range order, crystalline–amorphous core–shell Si NWs may have remarkable potential for improvement of absorption.[15] We have also previously reported black Ge on flexible substrates based on crystalline–amorphous core–shell NW arrays with minimal optical reflectance (<1%) even for high angles of incidence (~75°) and relatively short lengths (~1 μm).[16] Interestingly, Ge NWs grown in our previous study using nickel (Ni) as catalyst exhibited a tapered structure unlike the completely straight Ge

[a]Department of Materials Science and Engineering, National Tsing Hua University, 101 sec 2, Kuang-Fu Road, Hsinchu 30013 Taiwan, Republic of China. E-mail: ylchueh@mx.nthu.edu.tw

[b]Centre for High Impact Research, University of Malaya, Kuala Lumpur 50603, Malaysia

[c]Materials Engineering Program, Department of Mechanical Engineering, University of Malaya, Kuala Lumpur 50603, Malaysia

[d]Department of Physics, 206 Allison Laboratory, Auburn University, AL 36849, USA

[e]Department of Electrical Engineering and Computer Sciences, University of California at Berkeley, Berkeley, CA 94720, USA. E-mail: ajavey@berkeley.edu

† Electronic supplementary information (ESI) available: Complementary TEM micrographs show the temperature- and time-dependent growth of NWs. Additional figure as mentioned in the text. See DOI: 10.1039/c5ra00888c

NWs in earlier reports where gold (Au) was the catalyst.[17] The tapering effect in the case of Ni-catalyzed growth was hypothesized[16] to originate from the difference in the radial vapour deposition rate (a non-catalytic process) and the axial growth rate (a catalytic process governed by the NiGe system phase diagram), but the underlying mechanism of catalyst-dependent morphological evolution in crystalline–amorphous core–shell NWs has never been systematically examined. Most studies to date particularly deal with growth factors such as temperature, pressure or substrate and their effect on the orientation of NWs.[18] Manipulating the growth direction and taking advantage of crystallographic defects allows the development of complex morphologies *via* kinking and branching. However in the case of individual NWs, rather than hierarchical structures that are produced by branching, there are still contradicting views as to whether stacking faults originate the formation of kinking sites. The only systematic approach in this regard is that of Dick *et al.* who have demonstrated controlled kinking by insertion of an axial heterojunction based on island growth at the NW–catalyst interface in certain compositions.[19]

In this paper, we employ Ni, Au and iron (Fe) thin films as catalyst to grow Ge NWs with tapered, straight, spiral, and ring type morphologies. Experimental results are used to elucidate how tuning the axial rate of growth (R_a) *versus* the lateral rate of deposition of the amorphous layer (R_l) which in some cases can be asymmetric, leads to a wide range of stress-induced geometries. FEM simulations based on the modified Stoney's formula for thin films and more accurate MD calculations considering the non-uniform misfit strain distribution in the core–shell structure are also presented to confirm the proposed mechanism of deformation. The model established here can serve as a groundwork for development of engineered crystalline–amorphous core–shell NWs with promising applications in solar cells,[20] non-volatile crossbar switches,[21] and high-capacity battery electrodes.[22] Other relevant systems that may benefit from the model presented here, are metal-catalyzed Si–Ge core–shell heterostructures that have a similar growth behaviour and have been recently used to demonstrate 1D hole gas systems at room temperature.[23] Interfacial stress in these systems are also expected to enable band gap engineering that renders our work even more relevant.[24]

Experimental section

Initially a thin oxide layer was thermally grown on a silicon substrate. The metal catalyst thin film (Au ~ 30 nm, Ni ~ 0.5 nm or Fe ~ 100 nm) was then deposited on the oxide layer *via* thermal evaporation. Ge NWs were grown using GeH_4 (12 sccm, 10% balanced in H_2) as the precursor at a temperature range of 270–300 °C and pressure of 40–50 Torr. The nanostructures were examined by high-resolution transmission electron microscopy (HR-TEM, JEM-3000F, JEOL operated at 300 kV with point-to-point resolution of 0.17 nm) and element mapping was achieved by electron energy loss spectrum (EELS).

Results and discussion

A number of studies have demonstrated the feasibility of growing NWs through either VSS or vapour–liquid–solid (VLS) processes.[25,26] and more recently using supercritical-fluid–liquid–solid (SFLS) methods.[27] Morales and Lieber[28] have reported Ge NWs from FeGe seeds at 820 °C using VLS growth. In the present work in contrast, a low-temperature VSS growth at ~300 °C was employed in order to enable the use of polymeric substrates for flexible devices. Other than practical considerations, the low temperature provides an interesting environment for the growth of NWs. We have previously shown that the diameter of the crystalline core of NWs consistently expands with the growth temperature (also see Fig. S1†).[16] This behaviour can be attributed to an increase in size of XGe (X: metal catalyst) seeds at higher temperatures prior to axial growth and therefore in principle applies to any catalyst as also reported in earlier studies.[15,17] Hence, we can conclude that the growth mechanism behind the crystalline core in core–shell NWs is essentially a catalytic process while the rate at which the axial growth of the amorphous shell takes place, directly correlates with the properties of the intermediate binary phase.[29] A low growth temperature means that beyond a critical thickness of a few nanometres, the insufficient thermal energy can no longer sustain a VSS-assisted epitaxial growth and the strictly vapour–solid deposition of the amorphous shell dominates in the lateral direction. With the assumption that the direct vapour–solid deposition does not involve a catalytic process, we carried out several experiments to see how tuning the rate of axial growth and that of lateral deposition can be used to guide the evolution of NWs. As shown in the optical and scanning electron micrographs of Fig. 1, the NWs grown using Au catalyst (Fig. 1a) do not exhibit any significant morphological deformation whereas those grown *via* Ni catalyst have a

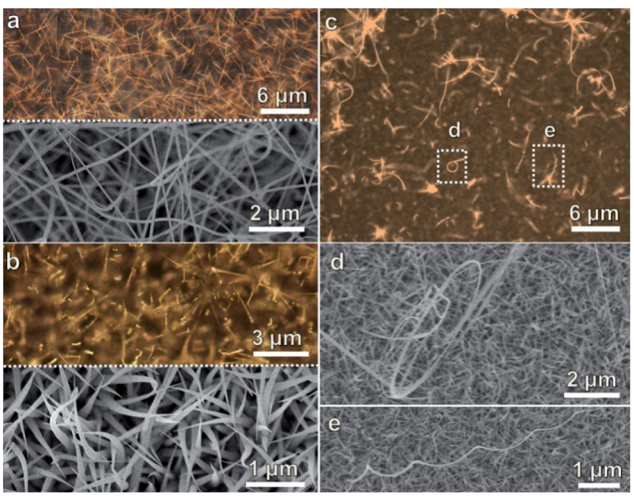

Fig. 1 Optical micrographs along with the corresponding scanning electron images of different NW morphologies at a temperature of 280 °C with a pressure of 40 Torr: straight NWs grown using Au (a), tapered NWs grown using Ni (b), and ring-like as well as spiral NWs grown using Fe (c–e).

tapered geometry (Fig. 1b). The case of Fe-catalyzed growth (Fig. 1c) is more interesting as the Ge NWs seem to have a tendency to bend either completely to give rise to ring type morphologies (Fig. 1d) or in a sinusoidal manner to create spiral structures (Fig. 1e).

A closer inspection using transmission electron microscopy (TEM) is depicted in Fig. 2. Fig. 2a indicates the core–shell configuration of the Ge NW grown from Au as the catalyst. The corresponding high-resolution TEM image of core–shell Ge NW as shown in Fig. 2b reveals that there is an amorphous shell layer along with a crystalline core made of pure Ge confirmed by selected area electron diffraction (SAED) pattern and energy dispersive X-ray (EDX) line scan as shown in Fig. 2c and d, respectively. Unlike the Au-catalyzed NWs which have a straight crystalline core, in the case of tapered Ge NWs grown using Ni at the catalyst, the core is considerably smaller with the increased length but at its widest point (at the base) has the same diameter as that of the NiGe seed shown in the inset of Fig. 2e. The Fe-catalyzed NWs on other hand mostly consist of a very thick amorphous shell. For spiral NWs, the shell deposition appears to uniformly alternate with the axial growth (Fig. 2f) whereas in the ring type structures (Fig. 2g), the amorphous layer (signified by wrinkles) is asymmetrically present only on the inner side along the ring (Fig. 2h and i). We can therefore categorize the morphology of NWs in terms of the catalytic axial growth rate (R_a) and the non-catalytic vapour–solid lateral deposition rate (R_l). With Au as the catalyst, the low eutectic point of AuGe alloy[30] promotes a faster axial growth as compared to the lateral deposition rate ($R_a \gg R_l$). Therefore, the NWs show no significant deformation. In Ni-catalyzed growth, the rate of catalytic growth is much slower than the rate of lateral deposition ($R_a \ll R_l$) because of the high melting point of NiGe alloy and the Ge NW tapering depends on slight differences in growth orientation regardless of the temperature and as a result, the crystalline core is considerably smaller than the amorphous shell. In the case of Fe on the contrary, due to the intermediate melting point of FeGe which is between those of NiGe and AuGe, the Ge NWs have a nearly equal catalytic growth and lateral deposition rates ($R_a \sim R_l$), hence the formation of spiral and complete ring morphologies.

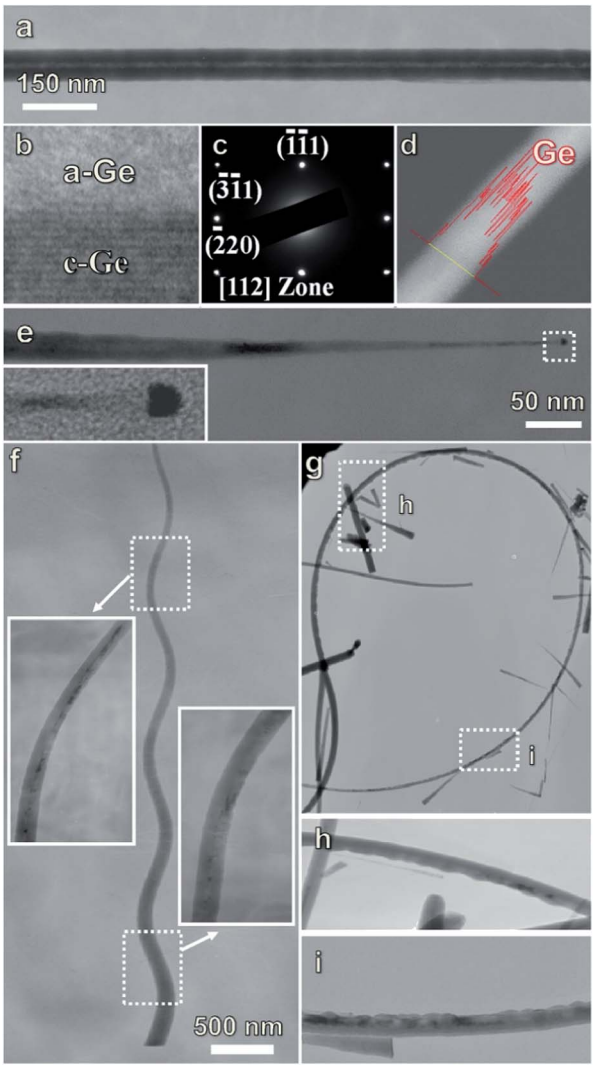

Fig. 2 TEM micrographs of different morphologies show the crystalline–amorphous core–shell structure. Straight NWs grown *via* Au catalyst exhibit a large crystalline core (a). The corresponding high-resolution TEM (b) and the SAED pattern (c) indicates an interplanar spacing of 3.2 nm attributed to the (111) growth direction. The EDX line (d) confirms the consistent composition of core–shell NWs. (e) The NWs grown using Ni as catalyst with a tapered structure and the NiGe seed (inset) are depicted. NWs grown from Fe thin film can either show spiral (f) or ring-like (g) morphologies. The latter is attributed to the asymmetric deposition of the amorphous layer on the inner side as signified by wrinkles (h and i).

It has to be emphasized here that explaining the kinetics of growth for different alloy seeds in terms of relative melting points is not against the proposed VSS mechanism. As Gamalski and colleagues[30] have also argued, the system of AuGe for example follows the more kinetically accessible path to form a liquid at very low temperatures (based on *in situ* observations at 240 °C), whereas speaking from a thermodynamic standpoint, there should not be a favourable path involving liquid below 360 °C (based on free-energy calculations for Au–Ge systems). They have concluded that kinetically-driven supersaturation determines the catalyst phase during the growth process. The reaction may start as a VLS-like growth with a metastable liquefaction of Au nanoparticles, however for most of the process it follows a VSS-type process and complete the reaction under solid–solid conditions rather than liquid–solid, hence the general analogy of VSS.

Overall, formation of different morphologies can be attributed to stress relaxation between the amorphous shell and the crystalline core. To support this notion, one can apply the standard Stoney's formula[31] to study the stress deformation in core–shell structures, for which the stress bearing of a thin film with uniform thickness h_f over a substrate of thickness h_s can be defined as

$$\sigma^{(f)} = \frac{E_s h_s{}^2 k}{6h_f(1-\nu_s)}$$

where the stress $\sigma^{(f)}$ of the film depends on the curvature k while ν and E, which are the Poisson's ratio and Young's modulus, respectively. The subscripts s and f represent the substrate and

thin film, respectively. However, this approach will not bear sufficiently reliable results for this particular case. Based on our observations, we have established that neither the assumption of thickness uniformity nor the equibiaxial in-plane stress are valid due to the intricate morphology. Furthermore, in the standard Stoney's formula, both shear stress and out-of-plane stress are not accounted for, a drawback which adds to its unreliability in our case.

Fortunately, in recent years, great progress have been made with regard to improving the original Stoney's equation by taking into account the minor effects that become increasingly more relevant in complex structures.[32–36] Freund and Suresh[37] have proposed a modified equation for non-uniform substrate and film curvatures, which can be written in cylindrical coordinates as

$$\sigma^{(f)} = \frac{E_s h_s^2 k}{6h_f(1-\nu_s)} \frac{d}{dr}(k_{rr} + k_{\theta\theta})$$

This modified equation provides a method for estimating the crystalline–amorphous interface shear stress with the radial gradient of the sum of the core and shell curvatures ($k_\Sigma = k_{rr} + k_{\theta\theta}$) and *COMSOL Multiphysics* was used to assess the stress-induced deformation in NWs based on the modified equation.[38] Fig. 3a–c show that the finite element model is in good agreement with the interfacial stress mechanism implied earlier from the experimental results. As expected, the straight NWs grown using Au-catalyzed VSS do not undergo any interfacial stress owing to the uniform coating of the amorphous shell layer around the crystalline Ge (Fig. 3a) while the tapered and spiral geometries clearly present residual stress due to their specific core–shell configuration (Fig. 3b and c). Although the FEM models account for the stress-induced curvature at the core–shell interface, they still do not represent the ratio of the laterally deposited amorphous shell against the axially grown crystalline core. Therefore, to offer a better insight into the process of deformation at the atomic scale, we need to apply a more comprehensive tool. Feng *et al.* have lately developed a new approach which expresses the stress gradient $\sigma_{rr}^{(f)} + \sigma_{\theta\theta}^{(f)}$ for the non-uniform misfit strain distribution corresponding to the non-uniform thickness of the core and the shell as[39]

$$\sigma_{rr}^{(f)} + \sigma_{\theta\theta}^{(f)} = \frac{E_s}{3(1-\nu_s^2)h_f}\left\{ h_s^2 k_\Sigma - \frac{1-\nu_s}{2} h_s^2 k_\Sigma + \frac{1}{2}\int_r^R [(1-3\nu_s)k_\Sigma(\eta) - 3(1-\nu_s)k_\Delta(\eta)]h_s^2(\eta)\frac{h_s'(\eta)}{h_{s0}}d\eta - \frac{1-\nu_s}{R^2}\int_0^R \eta^2[k_\Sigma(\eta) - k_\Delta(\eta)]h_s^2(\eta)\frac{h_s'(\eta)}{h_{s0}}d\eta \right\}$$

Similarly, the magnitude for this gradient is determined as

$$\sigma_{rr}^{(f)} - \sigma_{\theta\theta}^{(f)} = \frac{2E_f h_{s0}}{3(1+\nu_f)} k_\Delta$$

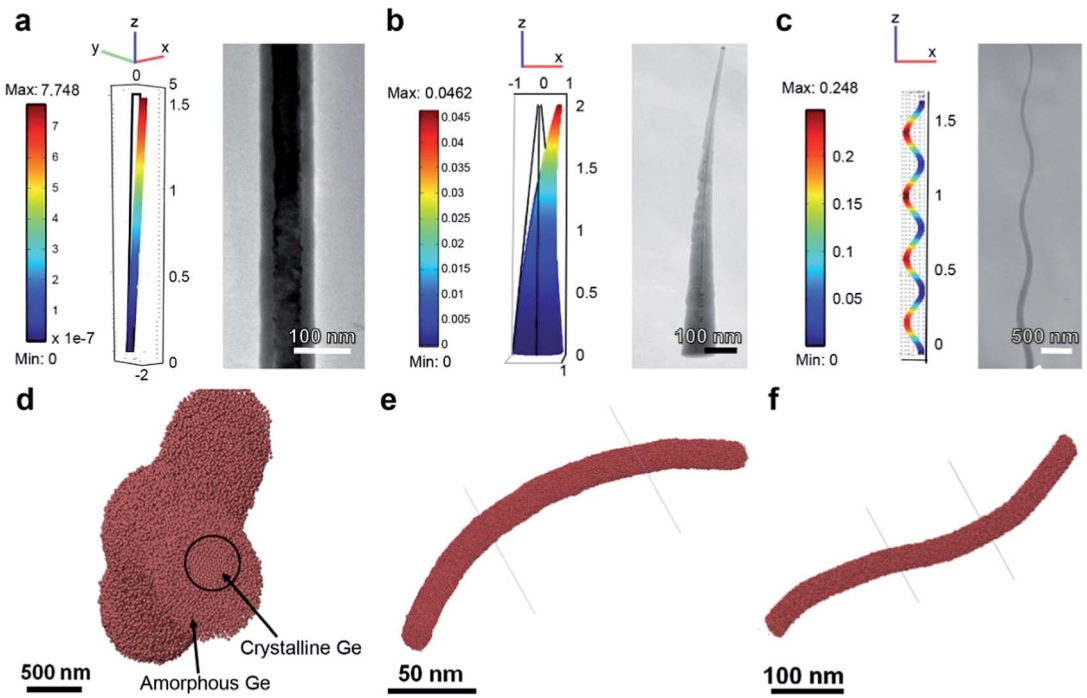

Fig. 3 FEM models of different NWs clearly demonstrate how interfacial stress gives rise to distinct morphologies (a–c). MD simulations clearly show the crystalline core against the amorphous shell in the cross-sectional image (d). Asymmetric and alternating vapour deposition of the amorphous shell leads to ring-type and spiral NWs, respectively.

Where ($k_\Delta = k_{rr} - k_{\theta\theta}$) is the differential curvature in the system, h_{s0} is a constant related to the substrate thickness and R is the radius of the boundary condition. The shear stress τ at the amorphous–crystalline interface is then given by

$$\tau = \frac{E_s}{6(1-\nu_s^2)}\left\{\frac{d}{dr}\left(h_s^2 k_\Sigma\right) - \frac{1}{2}\left[(1-3\nu_s)h_s^2 k_\Sigma - 3(1-\nu_s)h_s^2 k_\Delta\right]\frac{h_s'}{h_{s0}}\right\}$$

Subsequently, empirical parameters corresponding to the Ge core–shell were either taken from earlier studies[40,41] or derived from our experiments. Note that in order to reduce the computation time, MD simulations using LAMMPS were performed for reasonably scaled-down NWs as shown in Fig. 3d to f. Fig. 3d shows the cross section of a spiral NW where the perfectly crystalline core surrounded by the amorphous shell is clearly visible. Furthermore, by considering the non-uniform strain misfit distribution, we were able to study the effect of the core–shell thickness ratio on the abnormal deformation behaviour of Ge NWs grown from the Fe catalyst with the spiral geometry. Fig. 3e depicts the ring geometry as the lateral amorphous layer takes the form of an asymmetric coating while Fig. 3f presents a case of lateral amorphous layer in an alternating coating manner with the NW tending to bend into a spiral type morphology. The simulations accurately confirm our proposed model that the catalytic axial growth rate (R_a) and the non-catalytic lateral deposition rate (R_l) can be tuned to systematically change the morphology of crystalline–amorphous core–shell NWs.

Conclusions

We have thoroughly studied a systematic method for controlling the morphology of crystalline–amorphous core–shell NWs using interfacial stress. It was established that NW growth behaviour by metal catalysts closely correspond to the binary phase properties of the metal–semiconductor seed that in turn governs the rate of axial growth. On the other hand, a non-catalytic vapour–solid deposition in the lateral direction due to the low temperature of growth in a VSS process is responsible for the rate at which the amorphous shell is formed. The difference between axial and lateral growth rates can give rise to various morphologies from straight using Au ($R_a \gg R_l$), spiral using Fe ($R_a \sim R_l$), and tapered using Ni ($R_a \ll R_l$). Moreover, transformation of NWs into ring-like morphologies was found to be due to asymmetric deposition of the amorphous shell. The model proposed herein and additionally confirmed by FEM and MD simulations is expected to enable the growth of customized core–shell NWs with unique properties for electronic and optoelectronic applications.

Acknowledgements

This study is funded by the Ministry of Science and Technology through grant no. 101-2218-E-007-009-MY3, 103-2633-M-007-001, 101-2112-M-007-015-MY3, and National Tsing Hua University through Grant no. 104N2022E1. Researchers greatly appreciate the use of facility at CNMM the National Tsing Hua University through Grant no. 104N2744E1. A.Y. and C.C.T. acknowledge financial support under UM.C/625/1/HIR/237.

Notes and references

1 Y. Kayanuma, *Phys. Rev. B: Condens. Matter Mater. Phys.*, 1991, **44**, 13085–13088.
2 X. Peng, L. Manna, W. Yang, J. Wickham, E. Scher, A. Kadavanich and A. P. Alivisatos, *Nature*, 2000, **404**, 59–61.
3 W. S. Chiu, A. Yaghoubi, M. Y. Chia, N. H. Khanis, S. A. Rahman, P. S. Khiew and Y. L. Chueh, *CrystEngComm*, 2014, **16**, 6003–6009.
4 A. Yaghoubi and P. Mélinon, *Sci. Rep.*, 2013, **3**, 1083.
5 H. J. Fan, P. Werner and M. Zacharias, *Small*, 2006, **2**, 700–717.
6 J. Zhu, Z. Yu, G. F. Burkhard, C. M. Hsu, S. T. Connor, Y. Xu, Q. Wang, M. McGehee, S. Fan and Y. Cui, *Nano Lett.*, 2008, **9**, 279–282.
7 Q. Chen, G. Hubbard, P. A. Shields, C. Liu, D. W. Allsopp, W. N. Wang and S. Abbott, *Appl. Phys. Lett.*, 2009, **94**, 263118–263121.
8 J. Q. Xi, M. F. Schubert, J. K. Kim, E. F. Schubert, M. Chen, S. Y. Lin, W. Liu and J. A. Smart, *Nat. Photonics*, 2007, **1**, 176–179.
9 Y. Cui and C. M. Lieber, *Science*, 2001, **291**, 851–853.
10 B. Tian, X. Zheng, T. J. Kempa, Y. Fang, N. Yu, G. Yu, J. Huang and C. M. Lieber, *Nature*, 2007, **449**, 885–899.
11 L. Tang, S. E. Kocabas, S. Latif, A. K. Okyay, D. S. Ly-Gagnon, K. C. Saraswat and D. A. Miller, *Nat. Photonics*, 2008, **2**, 226–229.
12 W. S. Ho, Y. H. Dai, Y. Deng, C. H. Lin, Y. Y. Chen, C. H. Lee and C. W. Liu, *Appl. Phys. Lett.*, 2009, **94**, 261107–261110.
13 D. Wang, Q. Wang, A. Javey, R. Tu, H. Dai, H. Kim, P. C. McIntyre, T. Krishnamohan and K. C. Saraswat, *Appl. Phys. Lett.*, 2003, **83**, 2432–2434.
14 Y. Wu and P. Yang, *Chem. Mater.*, 2000, **12**, 605–607.
15 M. M. Adachi, M. P. Anantram and K. S. Karim, *Nano Lett.*, 2010, **10**, 4093–4098.
16 Y. L. Chueh, Z. Fan, K. Takei, H. Ko, R. Kapadia, A. A. Rathore, N. Miller, K. Yu, M. Wu, E. E. Haller and A. Javey, *Nano Lett.*, 2010, **10**, 520–523.
17 D. Wang, R. Tu, L. Zhang and H. Dai, *Angew. Chem., Int. Ed.*, 2005, **44**, 2925–2929.
18 S. A. Fortuna and X. Li, *Semicond. Sci. Technol.*, 2010, **25**, 024005–024021.
19 K. A. Dick, S. Kodambaka, M. C. Reuter, K. Deppert, L. Samuelson, W. Seifert, L. R. Wallenberg and F. M. Ross, *Nano Lett.*, 2007, **7**, 1817–1822.
20 M. M. Adachi, M. P. Anantram and K. S. Karim, *Sci. Rep.*, 2013, **3**, 1546.
21 Y. Dong, G. Yu, M. C. McAlpine, W. Lu and C. M. Lieber, *Nano Lett.*, 2008, **8**, 386–391.
22 L. F. Cui, R. Ruffo, C. K. Chan, H. Peng and Y. Cui, *Nano Lett.*, 2008, **9**, 491–495.
23 W. Lu, J. Xiang, B. P. Timko, Y. Wu and C. M. Lieber, *Proc. Natl. Acad. Sci. U. S. A.*, 2005, **102**, 10046–10051.

24 X. Peng and P. Logan, *Appl. Phys. Lett.*, 2010, **96**, 143119–143121.
25 K. A. Dick, *Prog. Cryst. Growth Charact. Mater.*, 2008, **54**, 138–173.
26 A. I. Persson, M. W. Larsson, S. Stenström, B. J. Ohlsson, L. Samuelson and L. R. Wallenberg, *Nat. Mater.*, 2004, **3**, 677–681.
27 X. Lu, J. T. Harris, J. E. Villarreal, A. M. Chockla and B. A. Korgel, *Chem. Mater.*, 2013, **25**, 2172–2177.
28 A. M. Morales and C. M. Lieber, *Science*, 1998, **279**, 208–211.
29 J. Hu, T. W. Odom and C. M. Lieber, *Acc. Chem. Res.*, 1999, **32**, 435–445.
30 A. D. Gamalski, J. Tersoff, R. Sharma, C. Ducati and S. Hofmann, *Nano Lett.*, 2010, **10**, 2972–2976.
31 G. G. Stoney, *Proc. R. Soc. London, Ser. A*, 1909, **82**, 172–175.
32 H. Lee, A. J. Rosakis and L. B. Freund, *J. Appl. Phys.*, 2001, **89**, 6116–6129.
33 T. S. Park and S. Suresh, *Acta Mater.*, 2000, **48**, 3169–3175.
34 Y. Huang, D. Ngo and A. Rosakis, *Acta Mech. Sin.*, 2005, **21**, 362–370.
35 Y. Huang and A. J. Rosakis, *J. Mech. Phys. Solids*, 2005, **53**, 2483–2500.
36 D. Ngo, Y. Huang, A. J. Rosakis and X. Feng, *Thin Solid Films*, 2006, **515**, 2220–2229.
37 L. B. Freund and S. Suresh, *Thin film materials: Stress, defect formation and surface evolution*, 2004, Cambridge University Press, New York.
38 *COMSOL Multiphysics User's Guide*, Version: September, 2005.
39 X. Feng, Y. Huang and A. J. Rosakis, *J. Appl. Mech.*, 2007, **74**, 1276–1281.
40 J. Tersoff, *Phys. Rev. B: Condens. Matter Mater. Phys.*, 1989, **39**, 5566–5568.
41 J. Tersoff, *Phys. Rev. B: Condens. Matter Mater. Phys.*, 1990, **41**, 3248.